ACS OMEGA

http://pubs.acs.org/journal/acsodf

Article

Constructing Hierarchically Porous N-Doped Carbons Derived from Poly(ionic liquids) with the Multifunctional Fe-Based Template for CO_2 Adsorption

Qirui Guo,* Chong Chen, Fangcheng Xing, Weizhong Shi, Jie Meng, Hui Wan, and Guofeng Guan*

Cite This: *ACS Omega* 2021, 6, 7186−7198

Read Online

ACCESS | Metrics & More | Article Recommendations | Supporting Information

ABSTRACT: Nitrogen-doped hierarchical porous carbons with a rich pore structure were prepared via direct carbonization of the poly(ionic liquid) (PIL)/potassium ferricyanide compound. Thereinto, the bisvinylimidazolium-based PIL was a desirable carbon source, and potassium ferricyanide as a multifunctional Fe-based template, could not only serve as the pore-forming agent, including metallic components (Fe and Fe_3C), potassium ions (etching carbon framework during carbonization), and gas generated during the pyrolysis process, but also introduce the N atoms to porous carbons, which were in favor of CO_2 capture. Moreover, the hierarchically porous carbon NDPC-1-800 (NDPC, nitrogen-doped porous carbon) had taken advantage of the highest specific surface area, exhibiting an excellent CO_2 adsorption capacity and selectivity compared with NDC-800 (NDC, nitrogen-doped carbon) directly carbonized from the pure PIL. Furthermore, its hierarchical porous architectures played an important part in the process of CO_2 capture, which was described briefly as follows: the synergistic effect of mesopores and micropores could accelerate the CO_2 molecules' transportation and storage. Meanwhile, the appropriate microporous size distribution of NDPC-1-800 was conducive to enhancing CO_2/N_2 selectivity. This study was intended to open up a new pathway for designing N-doped porous carbons combining both PILs and the multifunctional Fe-based template potassium ferricyanide with wonderful gas adsorption and separation performance.

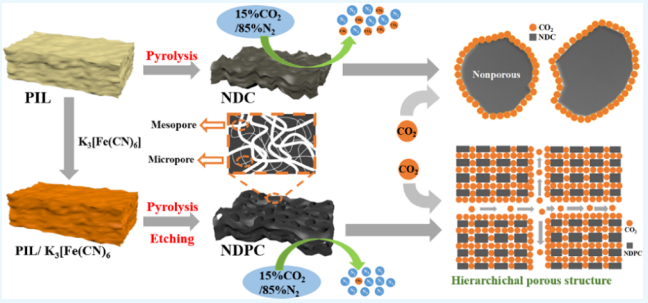

1. INTRODUCTION

Nitrogen-doped porous carbon (NDPC) has attracted great interest and is still an increasingly extending topic due to its tailorable pore texture, exceptionally larger surface area, lower density, as well as higher chemical and thermal stability.[1−5] Therefore, it has a wide application scope in the fields of adsorption, energy, catalysis, environment and separation, and so forth.[6−9] The general strategy to prepare porous carbon materials with large surface areas and the abundant pore structure can be summarized thus: hard or soft templates are applied in the carbonization process of a nitrogen-containing precursor.[10,11] However, this method still faces challenges in some degree. In simple terms, the removal of hard templates such as mesoporous silica suffers from the shortages of time- and energy-consuming procedures; besides, the soft templates may lose their structure at the high carbonization temperature; hence, this strategy goes against practical applications. Therefore, designing a sort of NDPC material with larger specific surface areas and high porosity together with simple and lower energy- and time-consuming approaches is still an essential issue to be researched.

Traditionally, nitrogen-doped carbon (NDC) materials were typically constructed by direct pyrolysis of nitrogen-containing organic compounds.[12−15] However, this approach usually suffers from either completely evaporating or decomposing into gaseous products of most organic precursors during the process of carbonization; thus, these traditional precursors are limited to natural or synthetic organics with low vapor pressures. Considering these issues of both low vapor pressures and complicated syntheses associated with organic precursors, a series of novel precursors have been reported by research workers as potential precursors of porous carbon materials, such as ionic liquids (ILs)[16,17] and metal organic frameworks.[18,19] ILs, as a novel kind of green materials together with their inappreciable vapor pressure and higher thermal stability, have received a substantial amount of attention as precursors of carbon materials.[16,20,21] These superior properties of ILs are beneficial for carbonization processes without any applied pressure, leading to minimizing mass loss before the start of the decomposition process; thus, we can obtain carbon material from direct carbonization. Moreover, the composition,

Received: January 22, 2021
Accepted: February 23, 2021
Published: March 3, 2021

Scheme 1. Preparation of the N-Doped Hierarchically Porous Carbon Derived from PIL and Potassium Ferricyanide

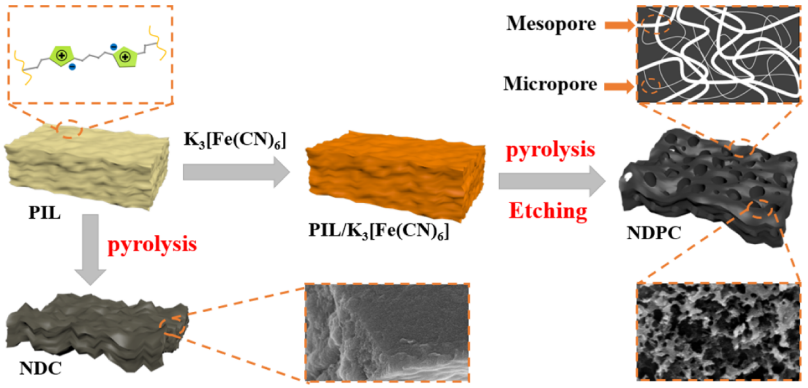

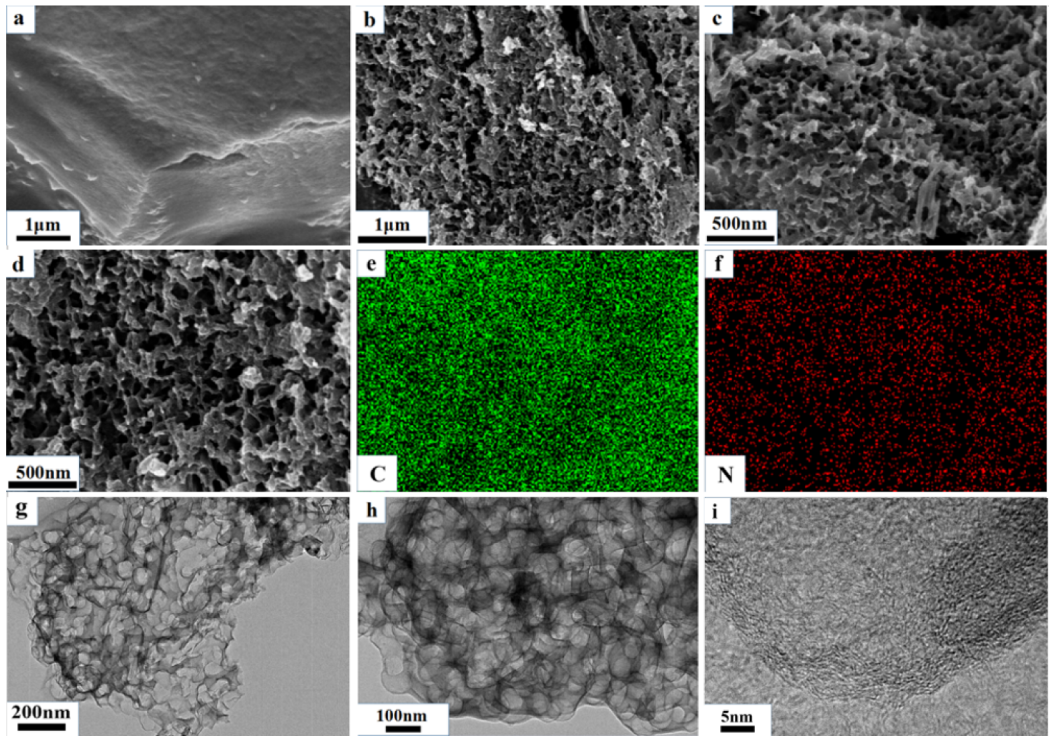

Figure 1. SEM images of NDC-800 (a) and NDPC-1-800 (b–d). EDS mapping images of C (e) and N (f) elements for NDPC-1-800 according to the corresponding SEM image (d). TEM images of NDPC-1-800 (g,h) and HRTEM image of NDPC-1-800 (i).

structure, and property of carbon materials can be tailored by the structural designability and compositional diversity of ILs.[21,22] Poly(ILs) (PILs), a kind of polymer solidified from IL monomers, exhibit outstanding properties of both ILs and macromolecule polymers.[23,24] The main advantages of using PILs as a unique class of carbon precursors are showed below. First, PILs, the same as ILs, have high thermal stability in order to minimize the mass loss and maximize the yields of carbon materials. Second, most PILs contain heteroatoms in their molecular structure such as nitrogen or sulfur, which can be preserved in a carbon matrix after carbonization, thus enhancing CO_2 uptake due to the improved affinity interaction between basic nitrogen active sites and acidic CO_2 molecules. Third, PILs, as solid materials, overcome the defects of ILs such as high viscosity and can be used conveniently in the process of carbonization. Consequently, PILs can be selected as the ideal carbon resources to prepare NDPCs, which are appropriate for CO_2 capture.

CO_2, as a predominant greenhouse gas and a renewable carbon resource, is supposed to be captured and stored effectively owing to global climate change and unreasonable usage of energy.[25−27] Alkaline amine-based solutions are currently utilized for CO_2 sorption by means of the chemical interaction between basic amino functional groups and acidic CO_2 molecules.[3,28] However, the shortages of this traditional method, such as equipment corrosion, chemical instability, and the high energy consumption of regeneration, worry the researchers.[29,30] In view of this, various adsorbents have been applied for CO_2 capture with high adsorption capacity.[31−33] Among them, NDPC is expected to be a promising CO_2 adsorbent because of its wide accessibility and a variety of advantages mentioned before.[34,35] As a result, developing a kind of porous carbons, which are suitable for CO_2 capture, is an attractive goal to be pursued.

In this work, we proposed a facile approach for preparing N-doped hierarchical porous carbon derived from a bisvinylimi-

https://dx.doi.org/10.1021/acsomega.1c00419
ACS Omega 2021, 6, 7186−7198

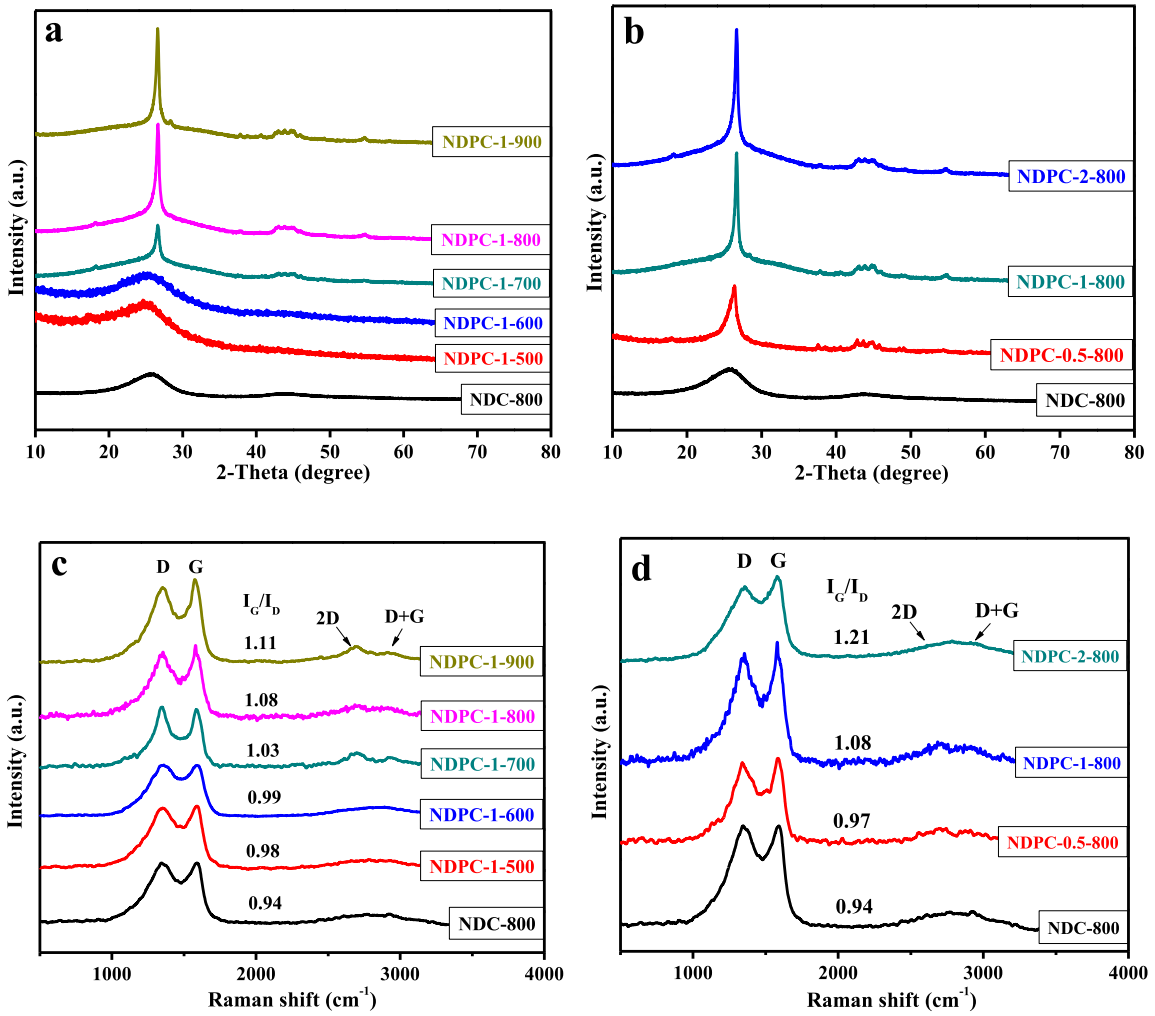

Figure 2. XRD patterns (a,b) and Raman spectra (c,d) of NDC-800 and NDPC-*x*-*y*.

dazolium-based PIL with potassium ferricyanide, subsequently removing the template with hydrochloric acid. The multifunctional Fe-based template potassium ferricyanide could provide not only the ferrous compounds, gas, and potassium ions for pore-forming during the pyrolysis process but also the N atoms to porous carbons, which were beneficial to CO_2 adsorption. The hierarchical porous carbon prepared at 800 °C had taken advantage of higher specific surface areas and well-developed porosity, exhibiting excellent adsorption performance compared with the carbon material directly carbonized from the pure PIL. Briefly, the mesopores could provide continuous channels for transporting CO_2 molecules; simultaneously, that of the microporous architecture would adsorb CO_2 molecules massively.

2. RESULTS AND DISCUSSION

The preparation route of our NDC materials is shown in Scheme 1. The hierarchical porous NDCs with abundant pore channels were obtained via a facile two-step process including the carbonization of the homogenized mixture (the pure PIL as an ideal carbon source and $K_3[Fe(CN)_6]$ as a multifunctional template) and the removal of the Fe-based template with hydrochloric acid subsequently. The diagrammatic drawing of an amplified portion on the porous carbon (NDPC) illustrated that the hierarchical structure of micropores and mesopores existed in this material, which further connected to those macropores finally. Furthermore, the NDC with hardly any pore structure was pyrolyzed directly from $P[C_4DVIM]Br_2$ in order to show the superiorities of $K_3[Fe(CN)_6]$.

The surface morphologies of NDC-800 and NDPC-1-800 were observed by SEM. As shown in Figure 1a, scarcely any pore structure could be visualized from NDC-800, which was directly carbonized from the pure PIL without potassium ferricyanide, and it corresponded precisely with the N_2 adsorption−desorption isotherms and pore size distribution of NDC-800 (Figure 3a,c). However, the shape of NDPC-1-800 was evidently distinguished from that of NDC-800. It could be seen from Figure 1b−d that the obtained NDPC-1-800 presented an interconnected framework with a rich pore structure. It was mainly owing to the gas and ferrous compounds originating from potassium ferricyanide during the process of carbonization and then acid-etching treatment to form the abundant pore channels. Moreover, the existence of K^+ during the carbonization process could also etch the carbon skeleton to construct more well-interconnected pore channels.[36,37] EDS mapping images of carbon and nitrogen (Figure 1e,f) in the selected NDPC-1-800 sample validated the homogeneous distribution of the doped N atoms on the surface of the porous carbon. The pore structure of NDPC-1-800 could be further confirmed from the TEM images. In Figure 1g,h, a large number of disordered macropores built up from carbonization and etching were observed clearly, and

https://dx.doi.org/10.1021/acsomega.1c00419
ACS Omega 2021, 6, 7186−7198

these porous channels provided CO_2 molecules more passageways to transport fast and conveniently. Moreover, the quite transparent nanosheets proved their highly porous textures. The high-resolution TEM (HRTEM) image (Figure 1i) revealed a curved nanosheet in NDPC-1-800, and that was in fact a graphite-like structure.

The ordered degree of carbon materials after thermal treatment was obtained by XRD patterns and is shown in Figure 2a,b. The appearance of two diffraction peaks at approximately 26 and 43° corresponded to the (0 0 2) and (1 0 0) planes of the graphitic carbons, respectively.[38,39] Meanwhile, it could be seen that a higher carbonization temperature or the existence of more potassium ferricyanide template during the process of carbonization resulted in a sharper and stronger (0 0 2) peak, indicating a higher graphitization degree.[40,41] Interestingly, the broad (0 0 2) peak became sharper and stronger obviously in Figure 2a once the temperature reached 700 °C, suggesting that a rapid graphitization process began at this temperature. In addition, the crystalline phases of metallic Fe and Fe_3C (JCPDS no. 06-0696 and 35-0772 respectively) could be tested in the XRD pattern of FNDPC-1-800 (FNDPC, Fe-containing nitrogen-doped porous carbon), the one without the removal of template (Figure S2), indicating that the major constituents of the template were both Fe and Fe_3C.

Raman spectroscopy was applied to further confirm the graphitic degree of the carbon materials, which were prepared at different pyrolysis temperatures (Figure 2c) or with different amounts of potassium ferricyanide (Figure 2d). The spectra showed that two intensive bands at about 1350 cm^{-1} (D band) and 1580 cm^{-1} (G band) corresponded to the defective carbon structure and the ordered structure of carbon with the sp^2 electronic configuration, respectively.[42,43] Usually, the degree of graphitization was estimated via the intensity ratio of the G/D band (I_G/I_D). Meanwhile, the value of I_G/I_D could also be influenced by the nitrogen content. Therefore, the I_G/I_D values of NDPC-*x*-*y* suggested that the higher pyrolysis temperature (I_G/I_D = 0.94−1.11) or the more potassium ferricyanide template amount (I_G/I_D = 0.94−1.21) would increase the graphitization degree gradually, which might be due to the change of nitrogen content at different conditions (Table 1).

The N_2 adsorption−desorption measurements were performed at 77 K to analyze the textural properties. The adsorption−desorption isotherms and corresponding pore size distributions of the carbon materials in this work are exhibited in Figure 3, and the results of Brunauer−Emmett−Teller (BET) specific surface areas (S_{BET}) and total pore volumes (V_{total}) are listed in Table 1. NDC-800, the carbon material carbonizing directly from the pure PIL at 800 °C, showed a nonporous structure that could be estimated from its S_{BET} and pore distribution, bearing a small S_{BET} value of 14 $m^2 \cdot g^{-1}$ and a low V_{total} (0.01 $cm^3 \cdot g^{-1}$). The isotherms of carbon samples carbonized at different temperatures with the mass ratio of the PIL/potassium ferricyanide = 1 are shown in Figure 3a. NDPC-1-500, 600 presented type-IV isotherms, suggesting the existence of mesopores with a few-micropore structure. Interestingly, when the temperature was at or higher than 700 °C, N_2 adsorption−desorption isotherms of these carbons transformed into type-I/IV with high adsorption capacities at low relative pressure (P/P_0 < 0.1) and exhibited more pronounced hysteresis loops, index of the structure involving micro-/mesopores.[44,45] The pore-forming of these hierarchically porous carbons was mainly attributed to the gas and Fe/Fe_3C templates originating from potassium ferricyanide during the process of carbonization and then acid-etching treatment with hydrochloric acid, while potassium ions could also etch the carbon framework during the process of pyrolysis. This result was in accordance with that in Table 1; the S_{BET} and V_{total} increased abruptly with 700 °C as the dividing line. The hierarchically porous structure of these carbon materials was conducive to CO_2 diffusion and adsorption that mesopores were used for transporting CO_2 molecules, while the micropores could offer plenty of space for accommodating the CO_2 molecules. This hierarchically porous structure could be further verified by pore size distributions.[23] The microporous size distribution curves were calculated by the Horvath−Kawazoe method, while the mesoporous size distribution curves were obtained through the Barrett−Joyner−Halenda method. It is clear that the peak values of these mesopores were located at approximately 3.7 nm, and the micropores were at the range of 0.54−0.81 nm, which was conducive to the CO_2/N_2 selectivity.[46] Meanwhile, the highest S_{BET} of the carbons above was achieved on the NDPC-1-800 sample (1189 $m^2 \cdot g^{-1}$). To investigate the influence of the different added amounts of potassium ferricyanide on the textural properties, the isotherms and pore size distributions of our carbons with different mass ratios of the PIL/potassium ferricyanide at 800 °C are depicted in Figure 3b,d,f, and the textural properties are listed in Table 1.

Elemental analyses were performed to access the element compositions of the carbon materials in this work, especially N content, which was beneficial to CO_2 capture.[47−49] As shown in Table 1, a common tendency of the decreasing N content from 16.84 to 1.87 wt % with the increasing pyrolysis temperature for carbon samples NDPC-1-*y* was observed. Among them, the N content of NDPC-1-800 was much lower than that of NDC-800, mainly due to the utilization of hydrochloric acid when removing templates. Notably, the N content of NDPC-1-700 decreased suddenly to 6.09 wt %, and the situation of this was similar to the corresponding values of textural properties, which might be related to the graphitic degree. Furthermore, the use of more potassium ferricyanide caused more nitrogen during preparation and it might be because potassium ferricyanide, as a multifunctional template, could provide not only the Fe-based templates Fe/Fe_3C for

Table 1. Textural Properties and Chemical Compositions of NDC-800 and NDPC-*x*-*y*

	textural property		chemical composition	
sample	S_{BET}[a] ($m^2 \cdot g^{-1}$)	V_{total}[b] ($cm^3 \cdot g^{-1}$)	C[c] (wt %)	N[d] (wt %)
NDC-800	14	0.01	84.75	8.81
NDPC-1-500	82	0.21	62.32	16.84
NDPC-1-600	257	0.39	65.48	15.78
NDPC-1-700	752	1.13	75.26	6.09
NDPC-1-800	1189	1.35	83.89	2.62
NDPC-1-900	447	0.46	89.18	1.87
NDPC-0.5-800	383	0.41	87.35	1.55
NDPC-2-800	640	0.96	83.32	2.77

[a]Specific surface areas were calculated by the BET method. [b]Total pore volumes were determined at P/P_0 = 0.99. [c]Carbon content was measured by elemental analysis. [d]Nitrogen content was measured by elemental analysis.

https://dx.doi.org/10.1021/acsomega.1c00419
ACS Omega 2021, 6, 7186−7198

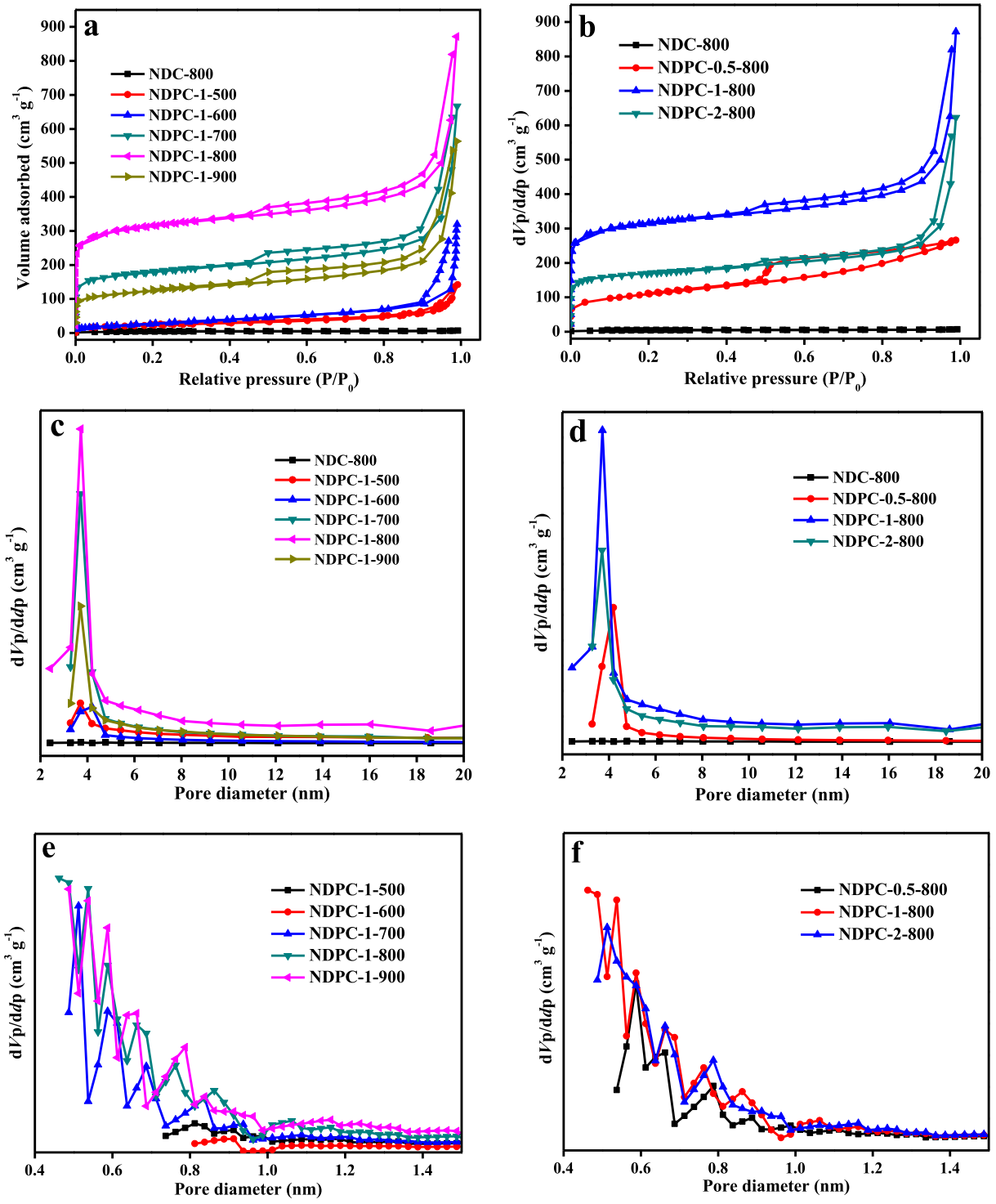

Figure 3. N_2 adsorption−desorption isotherms (a,b), mesoporous size distributions (c,d), and microporous size distributions (e,f) of NDC-800 and NDPC-*x*-*y*.

pore-forming but also the N atoms to porous carbons, which had interactions with acidic CO_2 molecules.

For better understanding the advantages of potassium ferricyanide templates, the porous carbon with the $FeCl_3$ template was synthesized at the same preparation conditions of NDPC-1-800 (shown in the Supporting Information), which was written as NDPC-$FeCl_3$. The textural properties and chemical compositions of these carbons are exhibited in Figure S3a and Table S1. It was clear that NDPC-$FeCl_3$ presented a micro-/mesoporous structure with a smaller S_{BET} of 539 $m^2 \cdot g^{-1}$, which was much smaller than that of NDPC-1-800. Moreover, the N content of NDPC-1-800 was higher than that of NDPC-$FeCl_3$, indicating that potassium ferricyanide could provide both Fe-based templates Fe/Fe_3C for pore-forming and N atoms. Meanwhile, the N content of composite FNDPC-1-800 (10.28 wt %) without the removal of the template could further confirm that potassium ferricyanide offered N atoms to carbon skeleton during pyrolysis.

https://dx.doi.org/10.1021/acsomega.1c00419
ACS Omega 2021, 6, 7186−7198

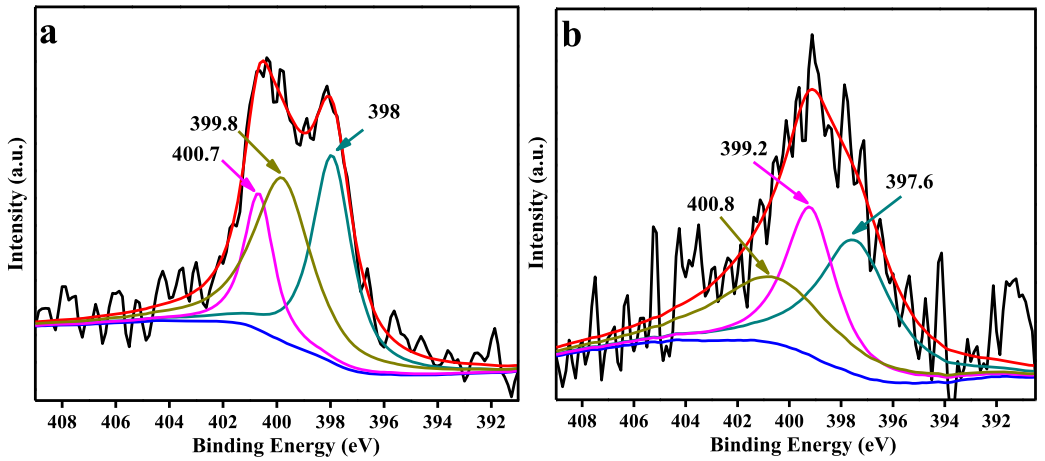

Figure 4. High-resolution N 1s XPS spectra of NDC-800 (a) and NDPC-1-800 (b).

XPS was carried out to investigate the binding environment of the nitrogen dopant in our carbon materials. Figure 4 exhibits the high-resolution N 1s spectra of NDC-800 (a) and NDPC-1-800 (b). The asymmetric N 1s peaks could be decomposed into three peaks mainly made up of pyridinic N (397.8 ± 0.2 eV), pyrrolic N (399.5 ± 0.3 eV), and graphitic-type quaternary N (400.7 ± 0.1 eV).[50,51] The N contents on the surfaces of NDC-800 and NDPC-1-800 tested by XPS were 6.60 and 2.78 wt %, respectively, which were almost the same as those (8.81 and 2.62 wt %) in the bulk materials detected by elemental analyses, indicating a uniform dispersion of N atoms, and the result was well coincident with the EDS elemental mapping analysis (see Figure 1f). Moreover, relatively more pyridinic and pyrrolic nitrogen inferred from the N 1s XPS spectra existed in these two carbons, which were in favor of CO_2 capture.[52] Meanwhile, it could be seen obviously from Figure S4 that the content of graphitic N increased during the pyrolysis process with potassium ferricyanide, which meant the increasing graphitic degree, and it was well in line with the result of the Raman spectrum.

The CO_2 adsorption isotherms of as-prepared carbon materials are depicted in Figure 5 with values between 10.32 and 34.65 $cm^3 \cdot g^{-1}$ measured at 25 °C and 1.0 bar. The CO_2 uptakes of as-prepared carbons increased steadily following increasing CO_2 pressure up to 1.0 bar, indicating that more CO_2 adsorption capacity could be achieved at higher pressures. In Figure 5a, the carbon derived from the pure PIL at 800 °C exhibited a lower CO_2 uptake of 10.32 $cm^3 \cdot g^{-1}$ at 25 °C and 1.0 bar despite its high N content (8.81 wt %). Although acidic CO_2 molecules could interact with the nitrogen atoms on the outer surface of NDC-800, hardly any pore channels existed. After thermal treatment and template removal of potassium ferricyanide, the amount of CO_2 sorption increased along with the temperature used for carbonization until 800 °C (34.65 $cm^3 \cdot g^{-1}$), and the tendency of increasing CO_2 uptake seemed good in relation to those of the BET specific surface areas. However, at a higher temperature of 900 °C, the CO_2 adsorption capacity declined sharply, even lower than that of NDPC-1-500, and the reason was not only the decreasing BET specific surface area but also the much lower nitrogen content (1.87 wt %). Usually, the doped nitrogen interacted with the acidic CO_2 molecules readily. Meanwhile, the CO_2 sorption isotherms of carbons with different amounts of potassium ferricyanide at 800 °C are exhibited in Figure 5b. It could be observed that the adsorption capacity of NDPC-1-800 was higher than those of both NDPC-0.5-800 and NDPC-2-800, suggesting that the biggest CO_2 adsorption capacity was presented when the mass ratio of $K_3[Fe(CN)_6]$/PIL = 1 due to its highest S_{BET} and hierarchically porous structure. The carbon materials derived from the bisvinylimidazolium-based PILs with the multifunctional template potassium ferricyanide exhibited higher CO_2 adsorption capacities than the non-porous carbon NDC-800, principally because its hierarchical porous architecture played an important part in the process of CO_2 adsorption, briefly describing that CO_2 molecules could transport and diffuse effectively in their mesoporous channels and simultaneously be adsorbed in micropores massively. Therefore, we could conclude that the CO_2 uptake of NDPC was determined by two significant factors: pore structure and nitrogen content.

The ideal adsorption solution theory (IAST) was applied to determine the CO_2/N_2 selectivity, which was crucial for practical applications.[53,54] In Figure 5d, the N_2 adsorption capacity of NDPC-1-800 was much lower than its CO_2 uptake rather than that of NDPC-1-800 in Figure 5c, indicating the high CO_2/N_2 selectivity of NDPC-1-800. Moreover, the dual-site Langmuir–Freundlich (DSLF) model was taken in Figure 5c,d for fitting the adsorption isotherms of CO_2 and N_2, which could describe these adsorptions more accurately.[55] The DSLF model (eq 1) is defined as follows.

$$q = q_1 \frac{b_1 p^{1/n_1}}{1 + b_1 p^{1/n_1}} + q_2 \frac{b_2 p^{1/n_2}}{1 + b_2 p^{1/n_2}} \quad (1)$$

q (mmol/g) herein was the equilibrium adsorption capacity at the corresponding pressure of p (kPa); q_i (mmol/g) and b_i (1/kPa) were the saturation capacity and the correlative coefficients for site i, respectively; and n_i was the deviation from the ideal surface. All the experimental data of NDC-800 and NDPC-1-800 were matched well with the fitting curves, indicative of the appropriate utilization of this model. The fitting parameters of DSLF are listed in Table 2. The CO_2/N_2 (15/85 v/v) selectivity was simulated from the flue gas mixture and the IAST as follows was picked to calculate the CO_2/N_2 selectivity (S_{ads}, eq 2).[54,56]

$$S_{ads} = \frac{q_{CO_2} P_{N_2}}{P_{N_2} q_{CO_2}} \quad (2)$$

https://dx.doi.org/10.1021/acsomega.1c00419
ACS Omega 2021, 6, 7186−7198

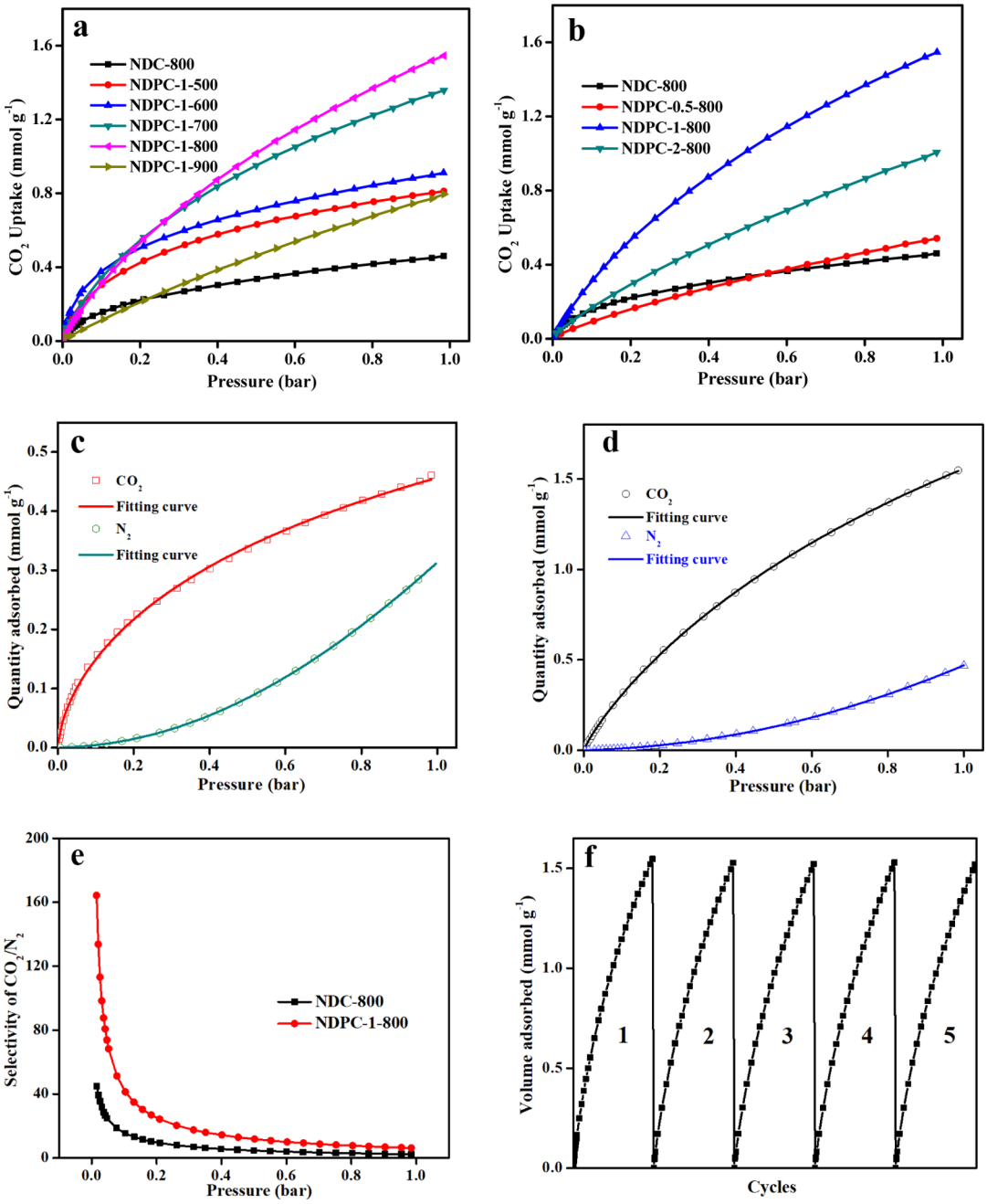

Figure 5. CO_2 adsorption isotherms of NDPC-1-*y* (a) and NDPC-*x*-800 (b) at 25 °C. The DSLF equation fitting of CO_2 and N_2 adsorption on NDC-800 (c) and NDPC-1-800 (d) at 25 °C (points, experimental data; lines, fitting curves). The CO_2/N_2 selectivities (e) on NDC-800 and NDPC-1-800 at 25 °C. Five consecutive cycles (f) of CO_2 adsorption−desorption on NDPC-1-800 at 25 °C and 1.0 bar.

Table 2. Fitting Parameters for the DSLF Isotherm Model

	NDC-800		NDPC-1-800	
	CO_2	N_2	CO_2	N_2
q_1 (mmol/g)	0.6142	3.5725	2.1881	0.7969
b_1 (1/kPa)	0.5915	0.0939	0.5522	0.1350
n_1	1.5886	0.4904	1.1574	0.8916
q_2 (mmol/g)	0.6142	0.1058	2.1881	5.0466
b_2 (1/kPa)	0.5915	0.0696	0.5522	0.0802
n_2	1.5886	1.4045	1.1574	0.4444
R^2	0.99912	0.99998	0.99996	0.99996

where S_{ads} represented the adsorption selectivity calculated by IAST, while q (mmol·g^{-1}) was the adsorption amount of the given gas in the equilibrium partial pressures of P (kPa). It is clear in Figure 5e that the selectivity of both NDC-800 and NDPC-1-800 decreased following the increasing pressure, and the CO_2/N_2 selectivity of NDPC-1-800 was always higher than that of NDC-800. At 0.1 bar, the CO_2/N_2 selectivity of NDPC-1-800 could reach 43.69, as much as around 3.1 times higher than that of NDC-800. Meanwhile, the CO_2/N_2 selectivity of NDPC-1-800 was still up to 8.23, whereas that of NDC-800 was only 2.32. It was mainly due to the advantages of both pore structure and N active sites of NDPC-1-800. In brief, the high selectivity of CO_2/N_2 was dependent on its high specific surface area; the tailored microporous structure peaked at 0.54 nm and the strong interaction with acidic CO_2 molecules.[46] However, NDC-800, which owned a nonporous structure,

https://dx.doi.org/10.1021/acsomega.1c00419
ACS Omega 2021, 6, 7186−7198

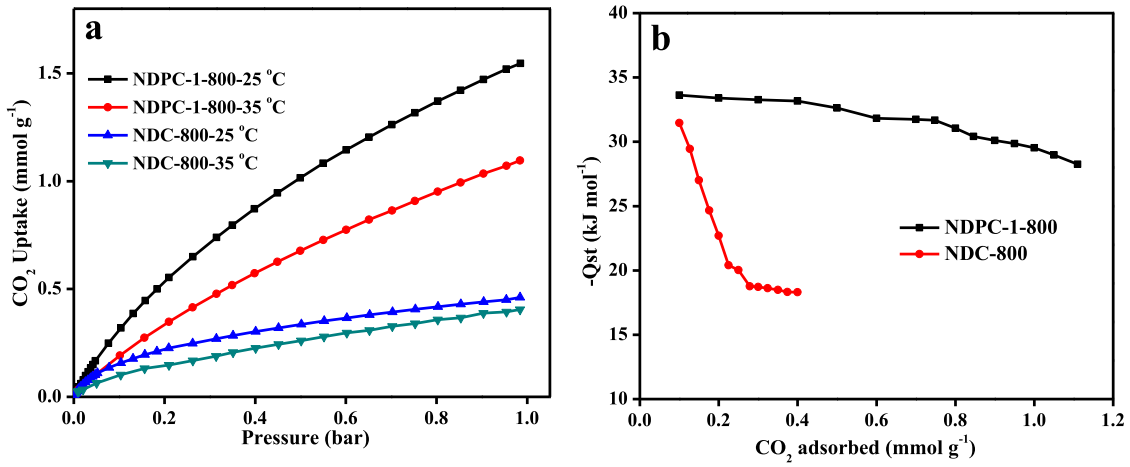

Figure 6. CO_2 adsorption isotherms (a) of NDC-800 and NDPC-1-800 at 25 and 35 °C. Isosteric heats of CO_2 adsorption (b) on NDC-800 and NDPC-1-800.

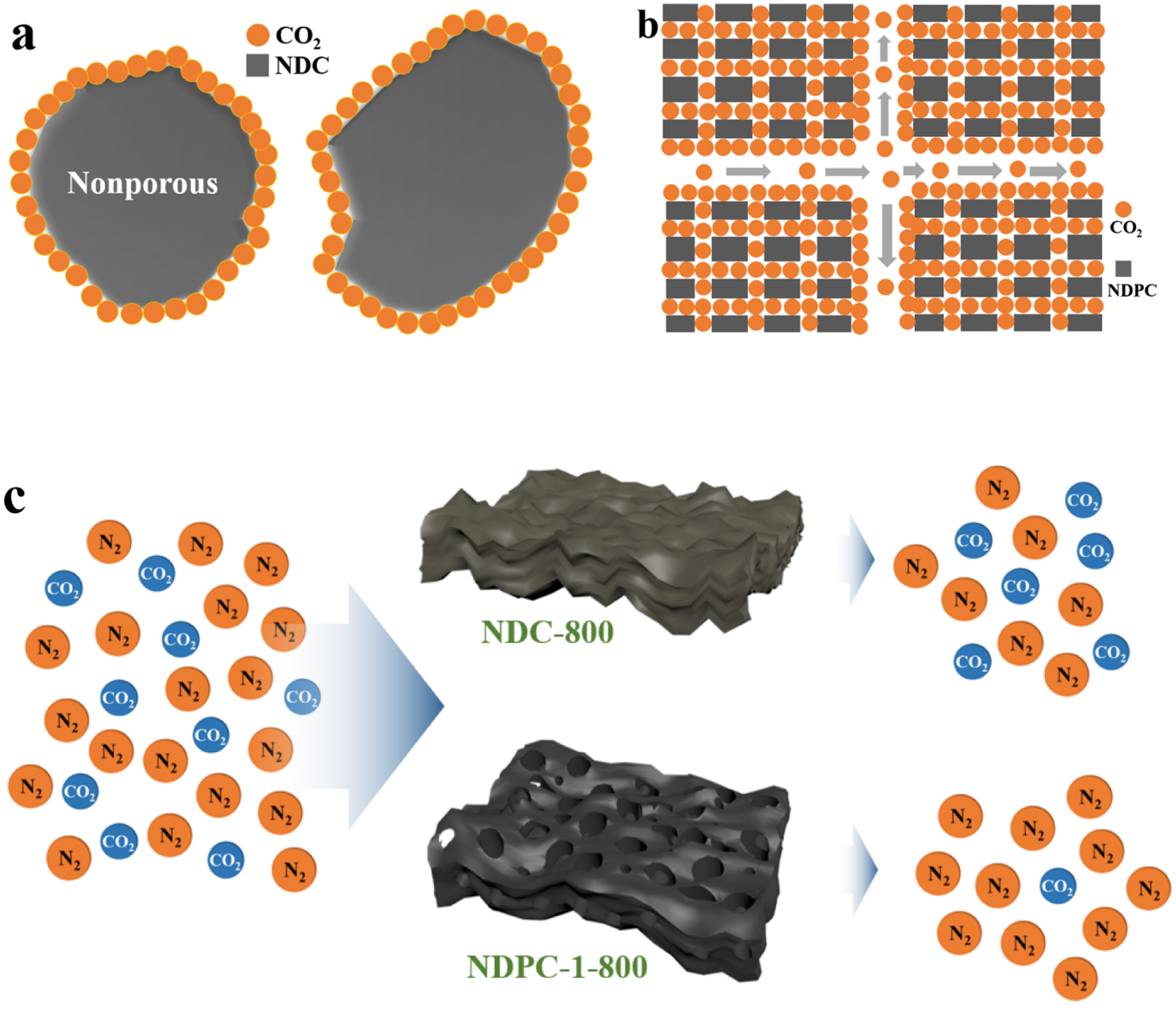

Figure 7. Mechanism diagram of CO_2 adsorption on NDC (a) and NDPC (b) adsorbents. Mechanism diagram of CO_2/N_2 selectivity (c) on NDC-800 and NDPC-1-800.

https://dx.doi.org/10.1021/acsomega.1c00419
ACS Omega 2021, 6, 7186−7198

could be only effected by its N active sites. The high CO_2 uptake and CO_2/N_2 selectivity made NDPC-1-800 a potential candidate adsorbent for solving environmental issues.

In consideration of practical applications, the selectivities of CO_2 adsorption from complicated conditions were further discussed. The CO_2/N_2 selectivities with different temperatures and CO_2 volume ratios were further investigated, and these related results are shown in Figure S5 and Table S2. In Figure S5b, it was clear that the CO_2/N_2 (15/85 v/v) selectivity of NDPC-1-800 at 25 °C was always higher than that of NDPC-1-800 at 35 °C (3.92), briefly due to the lower adsorption performance following the higher temperature. Subsequently, the CO_2/N_2 selectivities with different CO_2 volume ratios (10/15/20%) at the temperature of 25 °C were studied and are shown in Figure S5c. The DSLF model and corresponding fitting parameters are also exhibited in Figure 5d and Table 2. It could be observed that the CO_2/N_2 selectivity decreased following the increasing CO_2 volume ratio (from 11.18 to 5.26).

The regeneration capability of a CO_2 adsorbent was important for practical applications as well, and the reversibility of CO_2 adsorption−desorption on NDPC-1-800 was measured over five cycles at 25 °C and 1.0 bar. The sample was activated at 120 °C for 6 h under vacuum in order to make sure that the adsorbed CO_2 molecules could be removed thoroughly. In Figure 5f, no evident decrease in CO_2 uptake could be observed after five cycles, indicative of the good regenerability of our carbon material NDPC-1-800 with maintained stability.

To investigate the strength of interaction between the adsorbents and CO_2 molecules, the isosteric heat of adsorption (Q_{st}) was calculated by the CO_2 adsorption isotherms at 25 and 35 °C with the Clausius−Clapeyron equation (eq 3).[57,58] In Figure 6a, CO_2 isotherms of NDC-800 and NDPC-1-800 at 25 and 35 °C were presented to research the effect of CO_2 uptakes with temperature. Obviously, the CO_2 uptake of NDPC-1-800 decreased following the increasing temperature, indicating its physisorption process.[59] However, variation of temperature had little effect on the CO_2 adsorption capacity of NDC-800, mainly because most of the adsorbed CO_2 molecules on NDC-800 depended on the abundant N atoms of its outer surface with hardly any pore structure. Eq 3 was as follows.

$$P = -\frac{Q_{st}}{RT} + C \tag{3}$$

Equation 3 could be rewritten as shown below (eq 4) for convenient application.

$$Q_{st} = RT_1T_2\frac{\ln(P_2/P_1)}{T_2 - T_1} \tag{4}$$

Q_{st} (kJ·mol^{-1}) herein was the isosteric heat of CO_2 adsorption, R was the universal gas constant of 8.314 kJ·mol^{-1}·K^{-1}, and P_i (Pa) was the pressure at the temperature of T_i (K). In Figure 6b, the Q_{st} value of NDC-800 was about 31 kJ·mol^{-1} at a low surface coverage and decreased sharply to 18 kJ·mol^{-1} at a high surface coverage. The reason for this situation was that NDC-800 would have a strong interaction between basic N active sites and acidic CO_2 molecules at low CO_2 loading without any pore structure. Meanwhile, the favorable binding sites were occupied at a higher CO_2 coverage. However, the Q_{st} values on NDPC-1-800 dropped gradually from 34 to 28 kJ·mol^{-1} and was always higher than that of NDC-800, suggesting a stable physisorption process and strong interaction with CO_2 molecules on NDPC-1-800. What is more, the high Q_{st} value of NDPC-1-800 contributed to enhance its CO_2/N_2 selectivity.

In Figure 7, we proposed a possible CO_2 adsorptive mechanism of NDC and NDPC based on the characterization analysis above and previous related studies,[23,60,61] together with the advantages of NDPC. The adsorptive behavior of NDC is illustrated in Figure 7a, wherein CO_2 molecules could only attach on the outer surfaces of NDC just owing to the nonporous structure and the interaction between acidic CO_2 molecules and basic nitrogen atoms on the surfaces of NDC. In other words, the CO_2 uptake of NDC with hardly any pore structure just depended on the N content outside the surface. Nevertheless, potassium ferricyanide, as a multifunctional template, was so important for the hierarchically porous structure and chemical compositions of these carbons. It could provide not only the gas and Fe-based templates Fe/Fe_3C for pore-forming but also the N atoms to porous carbons. The excellent CO_2 adsorption capacity of NDPC was determined by both N content and pore structure, especially its hierarchically porous structure. In Figure 7b, we could find that the existence of both mesoporous and microporous structures provided a convenient way to CO_2 diffusion and adsorption; briefly, mesopores were just like many tubes to transport CO_2 molecules and simultaneously micropores offered plenty of space for accommodating CO_2 molecules. Furthermore, CO_2 molecules could also adhere to the passageway walls because of the interaction between the acidic CO_2 molecules and the doped nitrogen atoms on the surfaces of NDPC. The diagram of CO_2/N_2 selectivity on NDC-800 and NDPC-1-800 is depicted in Figure 7c. The higher CO_2/N_2 selectivity of NDPC-1-800 was mainly owing to its high S_{BET}, appropriate microporous size distribution, and hierarchically porous structure. The large S_{BET} could provide more contact areas for the interaction between basic N active sites and acidic CO_2 molecules, while the micropores peaking at 0.54 nm was attributed to the enhanced selectivity of CO_2 over N_2. Meanwhile, its hierarchical porous structure was able to accelerate the CO_2 molecule transportation. Therefore, this hierarchical porous carbon could combine many superiorities of CO_2 capture and would be a promising candidate adsorption material for practical applications.

3. CONCLUSIONS

In conclusion, we proposed a facile approach for preparing N-doped hierarchical porous carbons with abundant pore channels. It had been known that the bisvinylimidazolium-based PILs were ideal carbon sources, while potassium ferricyanide, as a multifunctional template, could provide not only the gas and Fe-based compounds (metallic Fe and Fe_3C) for pore-forming during the pyrolysis process but also the N atoms to porous carbons. The use of more potassium ferricyanide during preparation caused a higher nitrogen content, which had interaction with acidic CO_2 molecules. Moreover, the existence of K^+ ions during the carbonization process could also etch the carbon skeleton to construct more well-interconnected pore channels. Interestingly, the phase structure of these NDPCs would be changed during carbonization of the PIL with this multifunctional template; generally, a higher pyrolysis temperature or more potassium ferricyanide amount increased the graphitization degree gradually. Meanwhile, the hierarchical porous carbon prepared at 800 °C

https://dx.doi.org/10.1021/acsomega.1c00419
ACS Omega 2021, 6, 7186−7198

(NDPC-1-800) had taken advantage of the highest specific surface area (1189 $m^2 \cdot g^{-1}$) and the biggest pore volume (1.35 $cm^3 \cdot g^{-1}$), exhibiting an excellent CO_2 adsorption capacity (34.65 $cm^3 \cdot g^{-1}$) compared with the carbon material directly carbonized from the pure PIL, around 3.36 times as much as that of NDC-800. The existence of a hierarchical porous structure was in favor of the process of CO_2 capture, wherein the mesopores could provide a continuous channel for transporting CO_2 molecules; simultaneously, the microporous structure would offer plenty of space for accommodating CO_2 molecules massively. For practical applications, this carbon could be regenerated and reused easily with almost no drop in CO_2 uptake after five cycles. We demonstrated a novel and facile method to prepare N-doped hierarchical porous carbons and made sure that this kind of carbon materials could solve not only the threat of environment but also the shortage of energy.

4. EXPERIMENTAL SECTION

4.1. Materials. 1,4-Dibromobutane, 1-vinylimidazole, methanol, azobis(isobutyronitrile) (AIBN), ethanol, dichloromethane, and potassium ferricyanide ($K_3[Fe(CN)_6]$) were bought from Aladdin Chemical Co. Toluene, diethyl ether, acetone, and hydrochloric acid were purchased from Shanghai Lingfeng Chemical Reagent Co. All analytical-grade chemicals and solvents were obtained from commercial sources and used without further purification.

4.2. Synthesis of IL [C_4DVIM]Br_2. The bisvinylimidazolium salt [C_4DVIM]Br_2 was conveniently obtained by reaction between 1,4-dibromobutane and 1-vinylimidazole.[62,63] In brief, 1,4-dibromobutane (4.32 g, 20 mmol) and 1-vinylimidazole (3.96 g, 42 mmol) were added in toluene (20 mL), and the solution was stirred at 90 °C for 24 h. After cooling to normal temperature, the crude product was washed five times with diethyl ether. Subsequently, the obtained product was dissolved in methanol with activated carbon and stirred overnight for further purification. The final [C_4DVIM]Br_2 could be gained by centrifugation, rotary evaporation, and following vacuum drying at 40 °C. The Scheme for the synthesis of IL [C_4DVIM]Br_2 is shown in Figure S1.

4.3. Synthesis of the PIL Material. The PIL was prepared via the free radical polymerization of [C_4DVIM]Br_2.[62,63] Typically, [C_4DVIM]Br_2 (1.11 g, 2.75 mmol), AIBN (0.04 g), and ethanol (25 mL) were placed in a three-necked flask. Subsequently, the above mixture was reacted at 78 °C for 20 h under an N_2 atmosphere. After cooling down to normal temperature, the suspension was washed three times with methanol and dichloromethane. The PIL material P-[C_4DVIM]Br_2 was finally obtained via vacuum drying for 2 h at 40 °C.

4.4. Synthesis of Nitrogen-Doped Hierarchically Porous Carbon Materials. First, 5 g of PIL and a defined amount of $K_3[Fe(CN)_6]$ were dispersed in 100 mL of acetone through magnetic stirring for 48 h at normal temperature in order to gain the uniform mixture of $K_3[Fe(CN)_6]$/PIL. The organic solid could be achieved by washing with acetone and following vacuum drying overnight at 40 °C. The $K_3[Fe(CN)_6]$ and PIL were mixed completely together in a $K_3[Fe(CN)_6]$/PIL mass ratio of 0.5, 1, or 2, and donated as PF-*x* (*x* = 0.5, 1, 2). Afterward, these composites PF-*x* were heated at a certain temperature for 4 h with a nitrogen flow rate of 50 mL/min under the heating rate of 5 °C/min and then cooled to normal temperature. The carbonized samples were donated as FNDPC-*x*-*y*, which represented iron-containing NDPC. The solid carbon product FNDPC-*x*-*y* was then stirred in the concentrated hydrochloric acid (37 wt %) overnight. Finally, NDPC NDPC-*x*-*y* could be obtained by washing with water several times until pH = 7 and vacuum drying overnight at 80 °C. For comparison, P[C_4DVIM]Br_2 was pyrolyzed with the same conditions as FNDPC-*x*-*y* and donated as NDC-*y*, where *x* represented the $K_3[Fe(CN)_6]$/PIL mass ratio and *y* was the pyrolysis temperature.

4.5. Characterization. SEM images were obtained from a HITACHI S-4800 field emission scanning electron microscope, and EDS was also provided with this equipment. TEM images were collected on a JEM-2100 (JEOL) electron microscope. Raman spectra were obtained from a Jobin Yvon (Laboratory RAM HR1800) confocal micro-Raman spectrometer. XRD measurements were performed with a SmartLab 9kW. N_2 adsorption−desorption measurements were performed on the BELSORP-MINI analyzer, and these samples would be pretreated at 120 °C for 6 h under vacuum. Element analyses were carried out with a CHNS elemental analyzer Vario EL cube to determine the N contents of the samples. The XPS spectrum was recorded on a PHI-5000 Versa Probe system.

4.6. CO_2 and N_2 Adsorption Measurement. CO_2 adsorption isotherms were obtained on the MicrotracBEL BELSORP-max at 25 °C and 35 °C under the low pressure of 0−1.0 bar, and a 0.1 g sample was pretreated at 120 °C for 6 h under vacuum before measurements. N_2 adsorption isotherms were obtained on the BELSORP-MINI analyzer at 25 and 35 °C under the low pressure of 0−1.0 bar; a 0.05 g sample was pretreated at 120 °C for 6 h under vacuum before measurements. A CO_2 adsorption cyclic performance test was carried out multiple times at 25 °C to research the reusability of these adsorbents. These samples were vacuumized at 120 °C for 6 h after each adsorption process to ensure that the adsorbed CO_2 could be removed fully.

■ ASSOCIATED CONTENT

Supporting Information

The Supporting Information is available free of charge at https://pubs.acs.org/doi/10.1021/acsomega.1c00419.

Synthesis of porous carbon materials with $FeCl_3$; synthesis of IL monomer [C_4DVIM]Br_2; XRD pattern of the carbon composite FNDPC-1-800 without the removal of the template; N_2 adsorption−desorption isotherms and CO_2 adsorption isotherms of NDPC-1-800 and NDPC-$FeCl_3$; pyridinic, pyrrolic, and graphitic N proportion comparison of NDC-800 and NDPC-1-800; DSLF equation fitting of CO_2 and N_2 adsorption on NDPC-1-800 at 35 °C; CO_2/N_2 selectivities on NDPC-1-800 with different temperatures and CO_2 volume ratios; textural properties and chemical compositions of NDPC-1-800, NDPC-$FeCl_3$, and FNDPC-1-800; and fitting parameters for the DSLF isotherm model of NDPC-1-800 at 35 °C (PDF)

■ AUTHOR INFORMATION

Corresponding Authors

Qirui Guo − *Jiangsu Provincial Key Laboratory of Coastal Wetland Bioresources and Environmental Protection, School of Chemistry and Environmental Engineering, Yancheng Teachers University, Yancheng 224007, P. R. China; State*

https://dx.doi.org/10.1021/acsomega.1c00419
ACS Omega 2021, 6, 7186−7198

Key Laboratory of Materials-Oriented Chemical Engineering, College of Chemical Engineering, Jiangsu National Synergetic Innovation Center for Advanced Materials, Jiangsu Collaborative Innovation Center for Advanced Inorganic Function Composites, Nanjing Tech University, Nanjing 210009, P. R. China; orcid.org/0000-0002-7153-0354; Phone: +86 515 88213885; Email: guoqr@yctu.edu.cn

Guofeng Guan − *State Key Laboratory of Materials-Oriented Chemical Engineering, College of Chemical Engineering, Jiangsu National Synergetic Innovation Center for Advanced Materials, Jiangsu Collaborative Innovation Center for Advanced Inorganic Function Composites, Nanjing Tech University, Nanjing 210009, P. R. China*; Phone: +86 25 83587198; Email: guangf@njtech.edu.cn

Authors

Chong Chen − *State Key Laboratory of Materials-Oriented Chemical Engineering, College of Chemical Engineering, Jiangsu National Synergetic Innovation Center for Advanced Materials, Jiangsu Collaborative Innovation Center for Advanced Inorganic Function Composites, Nanjing Tech University, Nanjing 210009, P. R. China*

Fangcheng Xing − *Jiangsu Provincial Key Laboratory of Coastal Wetland Bioresources and Environmental Protection, School of Chemistry and Environmental Engineering, Yancheng Teachers University, Yancheng 224007, P. R. China*

Weizhong Shi − *Jiangsu Provincial Key Laboratory of Coastal Wetland Bioresources and Environmental Protection, School of Chemistry and Environmental Engineering, Yancheng Teachers University, Yancheng 224007, P. R. China*

Jie Meng − *State Key Laboratory of Materials-Oriented Chemical Engineering, College of Chemical Engineering, Jiangsu National Synergetic Innovation Center for Advanced Materials, Jiangsu Collaborative Innovation Center for Advanced Inorganic Function Composites, Nanjing Tech University, Nanjing 210009, P. R. China; Research Institute, Sinopec Yangzi Petrochemical Company, Ltd., Nanjing 210048, P. R. China*

Hui Wan − *State Key Laboratory of Materials-Oriented Chemical Engineering, College of Chemical Engineering, Jiangsu National Synergetic Innovation Center for Advanced Materials, Jiangsu Collaborative Innovation Center for Advanced Inorganic Function Composites, Nanjing Tech University, Nanjing 210009, P. R. China*

Complete contact information is available at: https://pubs.acs.org/10.1021/acsomega.1c00419

Notes

The authors declare no competing financial interest.

■ ACKNOWLEDGMENTS

We would like to thank the National Natural Science Foundation of China (21878159, U19B2001), the Foundation from State Key Laboratory of Materials-Oriented Chemical Engineering, Nanjing Tech University (ZK201712), the Foundation from Jiangsu Provincial Key Laboratory of Coastal Wetland Bioresources and Environmental Protection (JKLBS2019011), and the Jiangsu Provincial Emergency Management Science and Technology Project (YJGL-TG-2020-10) for financial support.

■ REFERENCES

(1) Zhang, J.; Zhang, X.; Zhou, Y.; Guo, S.; Wang, K.; Liang, Z.; Xu, Q. Nitrogen-Doped Hierarchical Porous Carbon Nanowhisker Ensembles on Carbon Nanofiber for High-Performance Supercapacitors. *ACS Sustainable Chem. Eng.* **2014**, *2*, 1525−1533.

(2) Liu, X.; Culhane, C.; Li, W.; Zou, S. Spinach-derived porous carbon nanosheets as high-performance catalysts for oxygen reduction reaction. *ACS Omega* **2020**, *5*, 24367−24378.

(3) Wang, L.; Rao, L.; Xia, B.; Wang, L.; Yue, L.; Liang, Y.; Dacosta, H.; Hu, X. Highly efficient CO_2 adsorption by nitrogen-doped porous carbons synthesized with low-temperature sodium amide activation. *Carbon* **2018**, *130*, 31−40.

(4) Li, X.; Song, Y.; You, L.; Gao, L.; Liu, Y.; Chen, W.; Mao, L. Synthesis of highly uniform N-doped porous carbon spheres derived from their phenolic-resin-based analogues for high performance supercapacitors. *Ind. Eng. Chem. Res.* **2019**, *58*, 2933−2944.

(5) Liu, B.; Liu, Y.; Chen, H.; Yang, M.; Li, H. Oxygen and nitrogen co-doped porous carbon nanosheets derived from perilla frutescens for high volumetric performance supercapacitors. *J. Power Sources* **2017**, *341*, 309−317.

(6) Li, Q.; Guo, J.; Xu, D.; Guo, J.; Ou, X.; Hu, Y.; Qi, H.; Yan, F. Electrospun N-doped porous carbon nanofibers incorporated with NiO nanoparticles as free-standing film electrodes for high-performance supercapacitors and CO_2 capture. *Small* **2018**, *14*, 1704203.

(7) Shao, L.; Sang, Y.; Liu, N.; Liu, J.; Zhan, P.; Huang, J.; Chen, J. Selectable microporous carbons derived from poplar wood by three preparation routes for CO_2 capture. *ACS Omega* **2020**, *5*, 17450−17462.

(8) Chen, W.; Zhang, G.; Li, D.; Ma, S.; Wang, B.; Jiang, X. Preparation of nitrogen-doped porous carbon from waste polyurethane foam by hydrothermal carbonization for H_2S adsorption. *Ind. Eng. Chem. Res.* **2020**, *59*, 7447−7456.

(9) Geng, J.-C.; Xue, D.-M.; Liu, X.-Q.; Shi, Y.-Q.; Sun, L.-B. N-doped porous carbons for CO_2 capture: rational choice of N-containing polymer with high phenyl density as precursor. *AIChE J.* **2017**, *63*, 1648−1658.

(10) Sun, L.; Zhou, H.; Li, L.; Yao, Y.; Qu, H.; Zhang, C.; Liu, S.; Zhou, Y. Double soft-template synthesis of nitrogen/sulfur-codoped hierarchically porous carbon materials derived from protic ionic liquid for supercapacitor. *ACS Appl. Mater. Interfaces* **2017**, *9*, 26088−26095.

(11) Wang, P.; Zhang, G.; Chen, W.; Chen, Q.; Jiao, H.; Liu, L.; Wang, X.; Deng, X. Molten salt template synthesis of hierarchical porous nitrogen-containing activated carbon derived from chitosan for CO_2 capture. *ACS Omega* **2020**, *5*, 23460−23467.

(12) Fu, N.; Wei, H.-M.; Lin, H.-L.; Li, L.; Ji, C.-H.; Yu, N.-B.; Chen, H.-J.; Han, S.; Xiao, G.-Y. Iron nanoclusters as template/activator for the synthesis of nitrogen doped porous carbon and its CO_2 adsorption application. *ACS Appl. Mater. Interfaces* **2017**, *9*, 9955−9963.

(13) Kim, C.; Zhu, C.; Aoki, Y.; Habazaki, H. Exothermically efficient exfoliation of biomass cellulose to value-added N-doped hierarchical porous carbon for oxygen reduction electrocatalyst. *Ind. Eng. Chem. Res.* **2019**, *58*, 3047−3059.

(14) Borghei, M.; Laocharoen, N.; Kibena-Põldsepp, E.; Johansson, L.-S.; Campbell, J.; Kauppinen, E.; Tammeveski, K.; Rojas, O. J. Porous N,P-doped carbon from coconut shells with high electrocatalytic activity for oxygen reduction: alternative to Pt-C for alkaline fuel cells. *Appl. Catal., B* **2017**, *204*, 394−402.

(15) Liu, X.; Pang, H.; Liu, X.; Li, Q.; Zhang, N.; Mao, L.; Qiu, M.; Hu, B.; Yang, H.; Wang, X. Orderly porous covalent organic frameworks-based materials: Superior adsorbents for pollutants removal from aqueous solutions. *Innovation* **2021**, *2*, 100076.

(16) Yuan, J.; Giordano, C.; Antonietti, M. Ionic liquid monomers and polymers as precursors of highly conductive, mesoporous, graphitic carbon nanostructures. *Chem. Mater.* **2010**, *22*, 5003−5012.

(17) Sadjadi, S.; Akbari, M.; Heravi, M. M. Palladated nanocomposite of halloysite-nitrogen-doped porous carbon prepared from a novel cyano-/nitrile-free task specific ionic liquid: an efficient catalyst for hydrogenation. *ACS Omega* **2019**, *4*, 19442−19451.

(18) Shao, Y.; Zhang, J.; Du, Y.; Jiang, H.; Liu, Y.; Chen, R. Controllable structure and basic sites of Pd@N-doped carbon derived from Co/Zn-ZIFs: role of Co. *Ind. Eng. Chem. Res.* **2019**, *58*, 14678−14687.
(19) Wang, T.; Li, Y.; Li, H.; Shi, D.; Jiao, Q.; Zhao, Y.; Su, P.; Wang, W.; Wu, Q. Rational design of hierarchical structural CoSe@NPC/CoSe@CNT nanocomposites derived from metal-organic frameworks as a robust Pt-free electrocatalyst for dye-sensitized solar cells. *ACS Omega* **2020**, *5*, 26253−26261.
(20) Paraknowitsch, J. P.; Zhang, Y.; Wienert, B.; Thomas, A. Nitrogen- and phosphorus-co-doped carbons with tunable enhanced surface areas promoted by the doping additives. *Chem. Commun.* **2013**, *49*, 1208−1210.
(21) Chen, C.; Feng, N.; Guo, Q.; Li, Z.; Li, X.; Ding, J.; Wang, L.; Wan, H.; Guan, G. Surface engineering of a chromium metal-organic framework with bifunctional ionic liquids for selective CO_2 adsorption: synergistic effect between multiple active sites. *J. Colloid Interface Sci.* **2018**, *521*, 91−101.
(22) She, Y.; Lu, Z.; Ni, M.; Li, L.; Leung, M. K. H. Facile synthesis of nitrogen and sulfur codoped carbon from ionic liquid as metal-free catalyst for oxygen reduction reaction. *ACS Appl. Mater. Interfaces* **2015**, *7*, 7214−7221.
(23) Guo, Q.; Chen, C.; Zhou, L.; Li, X.; Li, Z.; Yuan, D.; Ding, J.; Wan, H.; Guan, G. Design of ZIF-8/ion copolymer hierarchically porous material: coordination effect on the adsorption and diffusion for carbon dioxide. *Microporous Mesoporous Mater.* **2018**, *261*, 79−87.
(24) Gong, J.; Lin, H.; Antonietti, M.; Yuan, J. Nitrogen-doped porous carbon nanosheets derived from poly(ionic liquid)s: hierarchical pore structures for efficient CO_2 capture and dye removal. *J. Mater. Chem. A* **2016**, *4*, 7313−7321.
(25) Hao, W.; Björnerbäck, F.; Trushkina, Y.; Oregui Bengoechea, M.; Salazar-Alvarez, G.; Barth, T.; Hedin, N. High-performance magnetic activated carbon from solid waste from lignin conversion processes. 1. Their use as adsorbents for CO_2. *ACS Sustainable Chem. Eng.* **2017**, *5*, 3087−3095.
(26) Nugroho, F. A. A.; Xu, C.; Hedin, N.; Langhammer, C. UV-visible and plasmonic nanospectroscopy of the CO_2 adsorption energetics in a microporous polymer. *Anal. Chem.* **2015**, *87*, 10161−10165.
(27) Datta, S. J.; Khumnoon, C.; Lee, Z. H.; Moon, W. K.; Docao, S.; Nguyen, T. H.; Hwang, I. C.; Moon, D.; Oleynikov, P.; Terasaki, O.; Yoon, K. B. CO_2 capture from humid flue gases and humid atmosphere using a microporous coppersilicate. *Science* **2015**, *350*, 302−306.
(28) Song, C.; Ye, W.; Liu, Y.; Huang, H.; Zhang, H.; Lin, H.; Lu, R.; Zhang, S. Facile preparation of porous carbon derived from industrial biomass waste as an efficient CO_2 adsorbent. *ACS Omega* **2020**, *5*, 28255−28263.
(29) Wan, H.; Que, Y.; Chen, C.; Wu, Z.; Gu, Z.; Meng, J.; Wang, L.; Guan, G. Preparation of metal-organic framework/attapulgite hybrid material for CO_2 capture. *Mater. Lett.* **2017**, *194*, 107−109.
(30) Ji, C.; Wang, Y.; Zhao, N. Synthesis of Cu-Al hydrotalcite-SBA-15 composites and CO_2 capture using the sorbent. *Appl. Surf. Sci.* **2019**, *481*, 337−343.
(31) Chen, J.; Yang, J.; Hu, G.; Hu, X.; Li, Z.; Shen, S.; Radosz, M.; Fan, M. Enhanced CO_2 capture capacity of nitrogen-doped biomass-derived porous carbons. *ACS Sustainable Chem. Eng.* **2016**, *4*, 1439−1445.
(32) Lee, W. R.; Hwang, S. Y.; Ryu, D. W.; Lim, K. S.; Han, S. S.; Moon, D.; Choi, J.; Hong, C. S. Diamine-functionalized metal−organic framework: exceptionally high CO_2 capacities from ambient air and flue gas, ultrafast CO_2 uptake rate, and adsorption mechanism. *Energy Environ. Sci.* **2014**, *7*, 744−751.
(33) Chen, C.; Li, B.; Zhou, L.; Xia, Z.; Feng, N.; Ding, J.; Wang, L.; Wan, H.; Guan, G. Synthesis of hierarchically structured hybrid materials by controlled self-assembly of metal-organic framework with mesoporous silica for CO_2 adsorption. *ACS Appl. Mater. Interfaces* **2017**, *9*, 23060−23071.
(34) Zhang, S.; Mandai, T.; Ueno, K.; Dokko, K.; Watanabe, M. Hydrogen-bonding supramolecular protic salt as an "all-in-one" precursor for nitrogen-doped mesoporous carbons for CO_2 adsorption. *Nano Energy* **2015**, *13*, 376−386.
(35) Zhao, J.; Wei, J.; Cai, D.; Cao, H.; Tan, T. Polyaspartic acid-derived micro-/mesoporous carbon for ultrahigh H_2 and CH_4 adsorption. *ACS Omega* **2020**, *5*, 10687−10695.
(36) He, X.; Geng, Y.; Qiu, J.; Zheng, M.; Zhang, X.; Shui, H. Influence of KOH/coke mass ratio on properties of activated carbons made by microwave-assisted activation for electric double-layer capacitors. *Energy Fuels* **2010**, *24*, 3603−3609.
(37) Wang, J.; Kaskel, S. KOH activation of carbon-based materials for energy storage. *J. Mater. Chem.* **2012**, *22*, 23710−23725.
(38) Qian, W.; Zhu, J.; Zhang, Y.; Wu, X.; Yan, F. Condiment-derived 3D architecture porous carbon for electrochemical supercapacitors. *Small* **2015**, *11*, 4959−4969.
(39) Zhang, P.; Song, X.; Yu, C.; Gui, J.; Qiu, J. Biomass-derived carbon nanospheres with turbostratic structure as metal-free catalysts for selective hydrogenation of o-chloronitrobenzene. *ACS Sustainable Chem. Eng.* **2017**, *5*, 7481−7485.
(40) Zhu, J.; Xu, D.; Wang, C.; Qian, W.; Guo, J.; Yan, F. Ferric citrate-derived N-doped hierarchical porous carbons for oxygen reduction reaction and electrochemical supercapacitors. *Carbon* **2017**, *115*, 1−10.
(41) Chen, A.; Yu, Y.; Lv, H.; Wang, Y.; Shen, S.; Hu, Y.; Li, B.; Zhang, Y.; Zhang, J. Thin-walled, mesoporous and nitrogen-doped hollow carbon spheres using ionic liquids as precursors. *J. Mater. Chem. A* **2013**, *1*, 1045−1047.
(42) Wu, T.; Wang, G.; Dong, Q.; Zhan, F.; Zhang, X.; Li, S.; Qiao, H.; Qiu, J. Starch derived porous carbon nanosheets for high-performance photovoltaic capacitive deionization. *Environ. Sci. Technol.* **2017**, *51*, 9244−9251.
(43) Hou, J.; Liu, Y.; Wen, S.; Li, W.; Liao, R.; Wang, L. Sorghum-waste-derived high-surface area KOH-activated porous carbon for highly efficient methylene blue and Pb(II) removal. *ACS Omega* **2020**, *5*, 13548−13556.
(44) Li, G.; Zhang, J.; Li, W.; Fan, K.; Xu, C. 3D interconnected hierarchical porous N-doped carbon constructed by flake-like nanostructure with Fe/Fe_3C for efficient oxygen reduction reaction and supercapacitor. *Nanoscale* **2018**, *10*, 9252−9260.
(45) Zhong, H.-x.; Wang, J.; Zhang, Y.-w.; Xu, W.-l.; Xing, W.; Xu, D.; Zhang, Y.-f.; Zhang, X.-b. ZIF-8 derived graphene-based nitrogen-doped porous carbon sheets as highly efficient and durable oxygen reduction electrocatalysts. *Angew. Chem., Int. Ed.* **2015**, *53*, 14235−14239.
(46) Zulfiqar, S.; Sarwar, M. I.; Mecerreyes, D. Polymeric ionic liquids for CO_2 capture and separation: potential, progress and challenges. *Polym. Chem.* **2015**, *6*, 6435−6451.
(47) Zhang, S.; Li, Z.; Ueno, K.; Tatara, R.; Dokko, K.; Watanabe, M. One-step, template-free synthesis of highly porous nitrogen/sulfur-codoped carbons from a single protic salt and their application to CO_2 capture. *J. Mater. Chem. A* **2015**, *3*, 17849−17857.
(48) Li, D.; Chen, Y.; Zheng, M.; Zhao, H.; Zhao, Y.; Sun, Z. Hierarchically structured porous nitrogen-doped carbon for highly selective CO_2 capture. *ACS Sustainable Chem. Eng.* **2016**, *4*, 298−304.
(49) Gong, J.; Antonietti, M.; Yuan, J. Poly(ionic liquid)-derived carbon with site-specific N-doping and biphasic heterojunction for enhanced CO_2 capture and sensing. *Angew. Chem., Int. Ed.* **2017**, *56*, 7557−7563.
(50) Qin, Q.; Liu, Y.; Shan, W.; Hou, W.; Wang, K.; Ling, X.; Zhou, Y.; Wang, J. Synergistic catalysis of Fe_2O_3 nanoparticles on mesoporous poly(ionic liquid)-derived carbon for benzene hydroxylation with dioxygen. *Ind. Eng. Chem. Res.* **2017**, *56*, 12289−12296.
(51) Guo, D.; Ding, B.; Hu, X.; Wang, Y.; Han, F.; Wu, X. Synthesis of boron and nitrogen codoped porous carbon foam for high performance supercapacitors. *ACS Sustainable Chem. Eng.* **2018**, *6*, 11441−11449.
(52) Chen, G.; Wang, X.; Li, J.; Hou, W.; Zhou, Y.; Wang, J. Direct carbonization of cyanopyridinium crystalline dicationic salts into

https://dx.doi.org/10.1021/acsomega.1c00419
ACS Omega 2021, 6, 7186−7198

nitrogen-enriched ultra-microporous carbons toward excellent CO_2 adsorption. *ACS Appl. Mater. Interfaces* **2015**, *7*, 18508−18518.
(53) Liu, X.; Qi, S.-C.; Peng, A.-Z.; Xue, D.-M.; Liu, X.-Q.; Sun, L.-B. Foaming effect of a polymer precursor with a low N content on fabrication of N-doped porous carbons for CO_2 capture. *Ind. Eng. Chem. Res.* **2019**, *58*, 11013−11021.
(54) Li, J.-R.; Yu, J.; Lu, W.; Sun, L.-B.; Sculley, J.; Balbuena, P. B.; Zhou, H.-C. Porous materials with pre-designed single-molecule traps for CO_2 selective adsorption. *Nat. Commun.* **2013**, *4*, 1538.
(55) Xu, F.; Yu, Y.; Yan, J.; Xia, Q.; Wang, H.; Li, J.; Li, Z. Ultrafast room temperature synthesis of GrO@HKUST-1 composites with high CO_2 adsorption capacity and CO_2/N_2 adsorption selectivity. *Chem. Eng. J.* **2016**, *303*, 231−237.
(56) Liu, X.; Xiao, Z.; Xu, J.; Xu, W.; Sang, P.; Zhao, L.; Zhu, H.; Sun, D.; Guo, W. A NbO-type copper metal−organic framework decorated with carboxylate groups exhibiting highly selective CO_2 adsorption and separation of organic dyes. *J. Mater. Chem. A* **2016**, *4*, 13844−13851.
(57) Chowdhury, S.; Balasubramanian, R. Three-dimensional graphene-based porous adsorbents for postcombustion CO_2 capture. *Ind. Eng. Chem. Res.* **2016**, *55*, 7906−7916.
(58) Chen, C.; Huang, H.; Yu, Y.; Shi, J.; He, C.; Albilali, R.; Pan, H. Template-free synthesis of hierarchical porous carbon with controlled morphology for CO_2 efficient capture. *Chem. Eng. J.* **2018**, *353*, 584−594.
(59) Chen, C.; Feng, N.; Guo, Q.; Li, Z.; Li, X.; Ding, J.; Wang, L.; Wan, H.; Guan, G. Template-directed fabrication of MIL-101(Cr)/mesoporous silica composite: Layer-packed structure and enhanced performance for CO_2 capture. *J. Colloid Interface Sci.* **2018**, *513*, 891−902.
(60) Zhao, G.; Huang, X.; Wang, X.; Wang, X. Progress in catalyst exploration for heterogeneous CO_2 reduction and utilization: a critical review. *J. Mater. Chem. A* **2017**, *5*, 21625−21649.
(61) Li, J.; Wang, X.; Zhao, G.; Chen, C.; Chai, Z.; Alsaedi, A.; Hayat, T.; Wang, X. Metal-organic framework-based materials: superior adsorbents for the capture of toxic and radioactive metal ions. *Chem. Soc. Rev.* **2018**, *47*, 2322−2356.
(62) Agrigento, P.; Beier, M. J.; Knijnenburg, J. T. N.; Baiker, A.; Gruttadauria, M. Highly cross-linked imidazolium salt entrapped magnetic particles-preparation and applications. *J. Mater. Chem.* **2012**, *22*, 20728−20735.
(63) Qin, L.; Wang, B.; Zhang, Y.; Chen, L.; Gao, G. Anion exchange: a novel way of preparing hierarchical porous structure in poly(ionic liquid)s. *Chem. Commun.* **2017**, *53*, 3785−3788.

https://dx.doi.org/10.1021/acsomega.1c00419
ACS Omega 2021, 6, 7186−7198